Journal of proteome research

Article

pubs.acs.org/jpr

Metabolomic Serum Profiling Detects Early-Stage High-Grade Serous Ovarian Cancer in a Mouse Model

Christina M. Jones,[†] María Eugenia Monge,[†,◆] Jaeyeon Kim,[‡,▽] Martin M. Matzuk,[‡,§,∥,⊥,#,▽] and Facundo M. Fernández*[,†,○]

[†]School of Chemistry & Biochemistry, Georgia Institute of Technology, 901 Atlantic Drive NW, Atlanta, Georgia 30332, United States

[‡]Department of Pathology & Immunology, [§]Department of Molecular and Cellular Biology, [∥]Department of Molecular and Human Genetics, [⊥]Department of Pharmacology, [#]Center for Drug Discovery, and [▽]Center for Reproductive Medicine, Baylor College of Medicine, One Baylor Plaza, Houston, Texas 77030, United States

[○]Institute of Bioengineering and Biosciences, Georgia Institute of Technology, 315 Ferst Drive, Atlanta, Georgia 30332, United States

Supporting Information

ABSTRACT: Ovarian cancer is a deadly disease killing more than any other gynecologic cancer. Nonspecific symptoms, combined with a lack of early detection methods, contribute to late diagnosis and low five-year survival rates. High-grade serous carcinoma (HGSC) is the most common and deadliest subtype that results in 90% of ovarian cancer deaths. To investigate metabolic patterns for early detection of this deadly ovarian cancer, *Dicer-Pten* double knockout (DKO) mice that phenocopy many of the features of metastatic HGSC observed in women were studied. Using ultraperformance liquid chromatography−mass spectrometry (UPLC−MS), serum samples from 14 early-stage tumor (ET) DKO mice and 11 controls were analyzed in depth to screen for metabolic signatures capable of differentiating early-stage HGSC from controls. Iterative multivariate classification selected 18 metabolites that, when considered as a panel, yielded 100% accuracy, sensitivity, and specificity for classification. Altered metabolic pathways reflected in that panel included those of fatty acids, bile acids, glycerophospholipids, peptides, and some dietary phytochemicals. These alterations revealed impacts to cellular energy storage and membrane stability, as well as changes in defenses against oxidative stress, shedding new light on the metabolic alterations associated with early ovarian cancer stages.

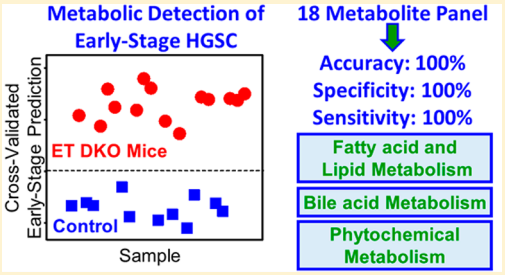

KEYWORDS: *ovarian cancer, mouse models, untargeted metabolomics, mass spectrometry, liquid chromatography, biomarkers, early detection*

INTRODUCTION

Ovarian cancer is the fifth leading cause of cancer-related deaths for U.S. women.[1] In particular, high-grade serous carcinoma (HGSC), the subtype with the highest occurrence and mortality, is responsible for 90% of all ovarian cancer deaths, yet its origin and early progression are poorly understood.[2−4] Because of the unavailability of reliable screening tests in clinical practice and the asymptomatic course through early stages of the disease, the majority of ovarian cancer cases (68%), including most HGSCs (>95%), are diagnosed as advanced, metastatic disease with poor survival.[5,6] The 5 year ovarian cancer survival rate for all cases diagnosed during 2002−2008 was 43%.[1] When the cancer is confined to the ovary at diagnosis, however, the 5 year survival is over 90%.[2] Early detection is thus crucial in reducing ovarian cancer mortality.

The conventional evaluation of patients includes physical examination, transvaginal ultrasonography, and measurement of levels of the serum tumor biomarker CA125. However, this marker is of limited utility because it can also be elevated by conditions unrelated to ovarian cancer, especially in premenopausal women.[7] Recent data[8,9] have suggested that the OVA1[10] test, the first protein-based *in vitro* diagnostic multivariate index assay (IVDMIA) approved by the FDA, may improve, along with physician clinical assessment, detection rates of malignancies among women with pelvic masses planning to undergo surgery. Nonetheless, whether this assay can detect HGSC at an early time point still remains unclear.[11]

During the past decade, metabolomics has emerged as a promising discipline providing tools to investigate characteristic metabolic patterns of disease, with one of its goals being the discovery of biomarker panels for early diagnosis. Mass spectrometry (MS) and ^{1}H nuclear magnetic resonance (NMR) spectroscopy in combination with multivariate statistical analysis have been utilized to investigate ovarian-cancer-induced metabolome alterations in urine,[12−15] plasma,[16,17] serum,[18−22] and tissues.[23−25] Li and collaborators, for example, identified L-tryptophan, lysoPC(18:3), lysoPC(14:0), and 2-piperidinone as

Received: September 19, 2014
Published: January 8, 2015

DOI: 10.1021/pr5009948
J. Proteome Res. 2015, 14, 917−927

plasma metabolites discriminating between epithelial ovarian cancer (EOC) patients and women with benign ovarian tumors.[16] Disruption to nucleotide, histidine, tryptophan, and mucin metabolism pathways[12,16] increased 27-nor-5β-cholestane-3,7,12,24,25 pentol glucuronide levels,[21] and changes in amino acids involved in *de novo* purine nucleotide synthesis have also been reported.[22] However, and despite these advances, no widely accepted strategy for metabolome-based ovarian cancer screening has yet emerged.[11,26] In addition to a lack of understanding of the early tumor development mechanisms accompanying disease progression, this is also due to the difficulty in obtaining sufficiently large, well-matched cohorts of early-stage ovarian cancer patients for further validation of metabolic changes reported in these various discovery studies.

Traditionally, ovarian cancer has been thought to originate in the ovary. The fallopian tube, however, has recently been proposed as an alternate site of origin, especially in women carrying hereditary *BRCA* mutations.[27−29] A mouse model of HGSC where disease originates through this alternative route was therefore developed by conditionally disabling two critical genes, *Dicer* and *Pten* (*Dicer* $^{flox/flox}$ *Pten* $^{flox/flox}$ *Amhr2* $^{cre/+}$), in the fallopian tubes.[30] In these *Dicer-Pten* double-knockout (DKO) mice, HGSCs originate and progressively develop in the fallopian tube before spreading to the ovary and then metastasize throughout the abdominal cavity, causing ascites, and eventually killing the mice. Besides replicating the clinical biology of human HGSC in that tumors are characterized by complex papillae and irregular glands forming slit-like spaces in addition to solid sheets of tumor cells with pleomorphic nuclei, prominent nucleoli, and elevated mitotic activity, disease in this DKO mice also shows close molecular similarities with human HGSCs, such as upregulated folate receptor 1 (*Folr1*), CA125 (*Muc16*), secreted phosphoprotein 1 (*Spp1*), and chemokine genes, therefore providing a simpler, better-controlled, model to study early-stage ovarian cancer, which could potentially be later translated to humans.

Here we report the first metabolomic profiling study of sera from *Dicer-Pten* DKO mice using ultraperformance liquid chromatography−mass spectrometry (UPLC−MS), showing that discrimination of early-stage tumor (ET) mice from controls with 100% accuracy, sensitivity, and specificity is possible through a panel of metabolite markers.

MATERIALS AND METHODS

Chemicals

Healthy human blood serum (S7023-50 mL) was purchased from Sigma-Aldrich (St. Louis, MO). FMOC-L-proline was procured from Chem-Impex International (Wood Dale, IL). Leucine enkephalin was obtained from ERA (Golden, CO). Arginyl-glycyl-aspartic acid, L-fucose, L-rhamnose, 1,5-anhydrosorbitol, D-fucose, L-rhamnulose, 2-deoxy-D-glucose, and 2-deoxy-D-galactose were acquired from Sigma-Aldrich Bilirubin, and suberic acid was obtained from Alfa Aesar (Ward Hill, MA). Ricinoleic acid was purchased from MP Biomedicals (Santa Ana, CA). Docosahexaenoic acid and 3-oxo stearic acid were acquired from Cayman Chemical Company (Ann Arbor, MI). LysoPE(16:0) was obtained from Avanti Polar Lipids (Alabaster, AL). LC−MS grade methanol was purchased from J.T. Baker Avantor Performance Materials (Center Valley, PA). Ultrapure water with 18.2 MΩ cm resistivity (Barnstead Nanopure, Thermo Fisher Scientific, Waltham, MA) was used to prepare chromatographic mobile phases.

Dicer-Pten Double-Knockout (Dicer-Pten DKO) Mice

Dicer-Pten DKO (*Dicer* $^{flox/flox}$ *Pten* $^{flox/flox}$ *Amhr2* $^{cre/+}$) mice were generated by mating males (*Dicer* $^{flox/flox}$ *Pten* $^{flox/flox}$ *Amhr2* $^{cre/+}$) with females (*Dicer* $^{flox/flox}$ *Pten* $^{flox/flox}$). Female *Dicer* $^{flox/flox}$ *Pten* $^{flox/flox}$ (a genotype not carrying *Amhr2* $^{cre/+}$) mice were used as controls.

Mice were housed in a vivarium with a controlled temperature of 21 °C. They were fed 5053 irradiated PicoLab Rodent Diet 20 and had access to drinking water supplied in bottles. *Dicer* $^{flox/flox}$ *Pten* $^{flox/flox}$ *Amhr2* $^{cre/+}$ DKO mice were sacrificed for this study in accordance to the animal protocol approved by the Institutional Animal Care and Use Committee (IACUC) at Baylor College of Medicine.

Serum Sample Collection

Blood samples were collected from 23 ET and 10 late-stage tumor (LT) *Dicer-Pten* DKO mice (*Dicer* $^{flox/flox}$ *Pten* $^{flox/flox}$ *Amhr2* $^{cre/+}$) in addition to 21 control mice (*Dicer* $^{flox/flox}$ *Pten* $^{flox/flox}$). Murine blood samples were collected into serum separator tubes. Serum was obtained by centrifugation at 14 000 rpm for 5 min at room temperature. Immediately after centrifugation, 200 μL serum aliquots were frozen and stored at −80 °C until UPLC−MS analysis.

Serum Sample Preparation and Experimental Design

Commercially available healthy human blood serum was used to optimize the serum sample metabolite extraction protocol and UPLC−MS method. Serum samples were thawed on ice prior to sample preparation. Methanol was added to 100 μL of each serum sample in a 3:1 ratio to precipitate proteins. Samples were vortex-mixed for 10 s and centrifuged at 13 000 rpm for 7 min. After centrifugation, 350 μL of supernatant was transferred to new microcentrifuge tubes and frozen at −80 °C for 2 h after the addition of 400 μL of ultrapure water. Subsequently, samples were lyophilized for 24 h at −50 °C and 25 mTorr using a VirTis benchtop freeze-dryer (SP Industries, Stone Ridge, NY). Sample residues were reconstituted in 100 μL of water/methanol (80:20 v/v, initial UPLC gradient conditions) and analyzed by UPLC−MS. Blank samples, consisting of ultrapure water, underwent the same process as murine serum samples. Samples were randomly separated into two batches and analyzed on consecutive days. Solvent and sample preparation blanks were jointly analyzed with murine serum samples. Quality control (QC) samples (15 μM FMOC-L-proline and leucine enkephalin solution in ultrapure water) were analyzed every 5 h to verify that retention time, peak shape, and intensity were stable for the duration of the analysis. The relative standard deviations of the retention times, peak areas, and intensities of the monoisotopic ions obtained from extracted ion chromatograms were <15% over the duration of the experiments.

Metabolic Profiling via Ultraperformance Liquid Chromatography−Mass Spectrometry

UPLC−MS analysis was performed using a Waters ACQUITY UPLC H Class system fitted with a Waters ACQUITY UPLC BEH C_8 column (2.1 × 100 mm, 1.7 μm particle size) and coupled to a Xevo G2 QTOF mass spectrometer (Waters, Manchester, U.K.) with a typical resolving power of 25 000 M/Δm fwhm and mass accuracy of 1.8 ppm at m/z 554.2615. The instrument was operated in negative ion mode with a probe capillary voltage of 2.5 kV and a sampling cone voltage of 45 V. The ion source and desolvation temperatures were 120 and 350 °C, respectively; the nitrogen desolvation flow rate was 800 L h^{-1}, and the cone desolvation flow rate was 50 L h^{-1}. The mass

DOI: 10.1021/pr5009948
J. Proteome Res. 2015, 14, 917−927

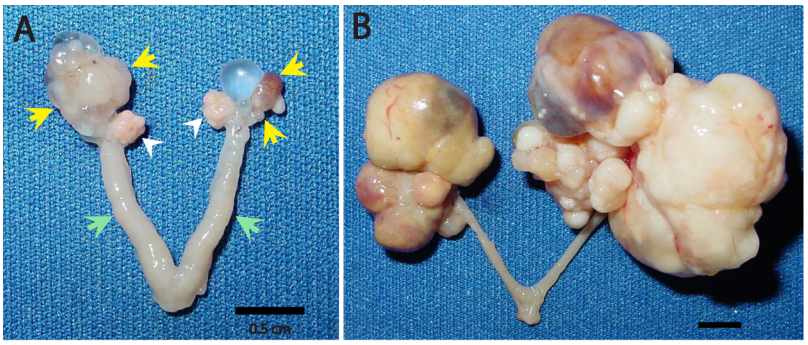

Figure 1. Early- and late-stage high-grade serous carcinomas (HGSCs) in DKO mice (*Dicer*$^{flox/flox}$ *Pten*$^{flox/flox}$ *Amhr2*$^{cre/+}$). (A) Early fallopian tube tumors (yellow arrows) formed in a 6.8 month old DKO mouse used in this study with normal ovaries (white arrowheads) and uterus (green arrows). (B) Massive fallopian tube tumors that engulfed the ovaries in a 10 month old DKO mouse with late-stage HGSCs.

spectrometer was calibrated across the 50−1200 m/z range using a 0.5 mM sodium formate solution prepared in 90:10 2-propanol/water v/v. Data were mass-corrected during acquisition using a leucine enkephalin reference spray (LockSpray) infused at 2 μL min^{-1}. Data were acquired in the 50−1200 m/z range, and the scan time was set to 1 s. Data acquisition and processing was carried out using MassLynx v4.1. The chromatographic method for sample analysis involved elution with water (mobile phase A) and methanol (mobile phase B) at a flow rate of 0.40 mL min^{-1} using the following gradient program: 0−15 min 20−90% B; 15−19 min 90% B. The gradient was returned to its initial conditions over a period of 11 min after each sample injection. The column temperature was set to 60 °C, the autosampler tray temperature was set to 5 °C, and the injection volume was 2 μL. Technical duplicates were acquired. UPLC−MS/MS experiments were performed by acquiring product ion mass spectra with applied voltages of 10, 20, and 30 V in the collision cell, using ultra-high-purity argon (≥99.999%) as the collision gas.

Data Analysis

Following UPLC−MS, spectral features (retention time (R_t), m/z pairs) were extracted from the data using MZmine 2.0 software.[32] This procedure involved chromatogram alignment, peak identification and integration, peak area extraction, and normalization after curation of the data matrix. The data matrix curation consisted of the removal of signals that were present in the blank samples, the solvent, or were not present in at least 50% of the serum samples. The curated data matrix was utilized to build a model for sample class discrimination via oPLS-DA and to down-select a smaller panel of discriminant features through the usage of a genetic algorithm (MATLAB version 7.13.0, The MathWorks, Natick, MA with PLS_Toolbox v.6.71, Eigenvector Research, Wenatchee, WA). A panel of 18 discriminant features had the lowest root-mean-square error of cross-validation (RMSECV) at the conclusion of the genetic algorithm variable selection process. The parameters for genetic algorithm variable selection were as follows: population size: 64, variable window width: 1, % initial terms (variables): 10, target minimum number of variables: 8, target maximum number of variables: 15, penalty slope: 0.05, maximum generations: 150, % at convergence: 79.7, mutation rate: 0.005, crossover: double, regression choice: PLS, number of latent variables: 6, cross-validation: random, number of splits: 5, number of iterations: 5, replicate runs: 20. PLS-DA models were orthogonalized and internally cross-validated using 10 iterations of random sample subsets with 5 data splits. Data were preprocessed by autoscaling prior to oPLS-DA analysis. Principal component analysis (PCA) was also performed to inspect data before and after genetic algorithm variable selection (i.e., on all of the extracted spectral features and only the discriminant feature panel).

Discriminant Feature Identification

Metabolite identification was attempted for the 18 discriminant features resulting from the genetic algorithm variable selection process. Mass spectral ion adduct analysis was first performed to ensure the unambiguous assignment of the signal of interest in each mass spectrum. The adduct ions that were investigated in the mass spectra included $[M-H]^-$, $[M+Cl]^-$, $[M+CH_3COO]^-$, $[M+HCOO]^-$, $[M+Na-2H]^-$, $[M+K-2H]^-$, $[M-H_2O-H]^-$, $[M+H_2O-H]^-$, and $[2M-H]^-$ species, which are usually observed in negative electrospray ionization mode. The theoretical m/z values for these species were calculated and compared with the experimental values from mass spectral signals. For spectra in which multiple adducts were not present, the accurate mass of the candidate neutral molecule was calculated based on the assumption that the m/z value observed corresponded to the $[M-H]^-$ ionic species. For mass spectra in which multiple adducts were present, the $[M-H]^-$ spectral signal was determined and the accurate mass of the metabolic candidate neutral molecule was calculated based on it. Elemental formulas were generated based on the exact mass (maximum mass error of 10 mDa) and isotopic patterns of the features using MassLynx 4.1. The elements included in the formulas were constrained to C, H, N, O, P, and S. The lists of generated elemental formulas were searched against the Metlin database,[33] the LIPID Metabolites and Pathways Strategy (LIPID MAPS) database,[34] and the human metabolome database (HMDB).[35] MetaboSearch[36] was also utilized to search the aforementioned databases solely using neutral masses with a mass accuracy of 20 ppm. Tandem MS data could not be acquired for discriminant features, where the precursor ion abundance was not high enough for sensitive quadrupole selection and MS/MS due to ion transmission losses.[37] The MS/MS Metlin database, MassBank,[38] and literature searches were used to further confirm the identity of the candidates for which MS/MS data were successfully acquired. Additionally, fragmentation patterns were manually analyzed in a few cases to discriminate between different isobaric species. Available chemical standards were purchased to validate tentative metabolite identities by chromatographic retention time matching or MS/MS fragmentation pattern matching. These chemical standards also served the purpose of eliminating possible metabolite candidates from the tentative identification list.

DOI: 10.1021/pr5009948
J. Proteome Res. 2015, 14, 917−927

RESULTS AND DISCUSSION

DKO Mouse Cohort

Typically, between 4 and 7 months, DKO mice develop high-grade serous carcinomas of the fallopian tubes, which later spread to envelop the ovaries and at a late stage metastasize throughout the abdominal cavity including peritoneal tissues (Figure 1). For the purpose of this study, early-stage tumors in DKO mice were defined as those confined to the fallopian tube without any sign of metastasis. Eventually, all DKO mice die from metastatic HGSCs after developing hemorrhagic ascites, an accumulation of hemorrhagic fluid in the abdominal cavity. The typical life span of these mice is 6.5−13 months.[30]

Initially, an exploratory experiment was conducted to determine to what extent UPLC−MS metabolic profiling could differentiate the blood sera of 9 ET (mean age 319 ± 36 days) and 10 LT (mean age 309 ± 34 days) DKO mice, in addition to 10 control (mean age 342 ± 80 days) mice. For this experiment, DKO mice were staged based on the presence or lack of ascites—LT DKO mice had developed ascites while ET DKO mice had not. Unsupervised PCA of the resultant data showed clear separation of LT DKO mice from ET DKO mice and control mice along the first principal component (unpaired t test, $n = 29$, $p = 0.002$) (Figure S1 in the Supporting Information). However, both ET DKO mice and control mice were clustered together. As expected, this result somewhat reflects what is clinically observed for the diagnosis of human ovarian carcinomas; that is, late stages in which metastasis has occurred are more easily detectable because the disease is systemically widespread, yet detection of early stages is challenging because the disease is still localized and asymptomatic.

In this stage the focus of the study was shifted to the detection of early stage HGSC in DKO mice by comparing metabolomic profiles between DKO mice with early stage HGSC against control mice, as this is the equivalent of the clinically relevant challenge for human HGSC detection. Therefore, a set of 14 *Dicer-Pten* DKO mice with early stage HGSC (mean age 206 ± 19 days) and 11 control mice (mean age 211 ± 30 days) was investigated via an alternative approach involving supervised multivariate analysis. ET DKO mice were sacrificed after blood sample collection to confirm the early tumor status by ensuring that all had primary tumors located on their fallopian tubes with no visible metastasis to ensure complete confidence in the class membership of each mouse in the cohort. Table S1 in the Supporting Information describes detailed information on the mice included in these experiments as well as the tumor status verified for each ET DKO mouse.

Multivariate Classification Performance

MZmine data processing extracted 934 features (R_t, m/z pairs) from the UPLC−MS data from both control and ET DKO mice (Data set S1 in the Supporting Information). These extracted features were utilized to build an oPLS-DA model that classified the respective serum samples from each class. Performance characteristics of the initial oPLS-DA analysis of the data matrix that included all 934 metabolic features (Figure 2A,B) were 76, 68, and 83% for the cross-validated accuracy, sensitivity, and specificity, respectively. A total of five murine serum samples were misclassified. This three latent variable model interpreted 35.35 and 93.64% variance from the X- (feature peak areas) and Y- (mouse class membership) blocks, respectively. Although the model performance was not entirely poor, genetic algorithms were used to attain a smaller, but more robust, metabolic feature set that could serve to better discriminate between control and

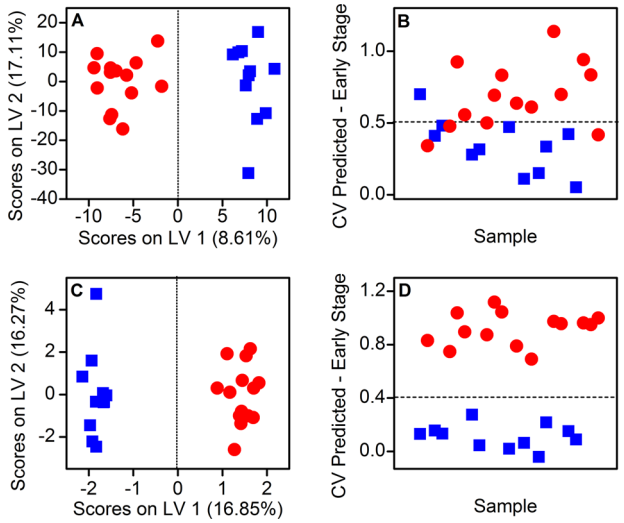

Figure 2. Orthogonal projection to latent structures-discriminant analysis (oPLS-DA) models of early stage tumor (ET) *Dicer-Pten* DKO (red circles) versus control mice (blue squares). (A) oPLS-DA calibration scores plot using the total initial set of 934 spectral features. The model consisted of three LVs with 35.35 and 93.64% total captured X- and Y-block variances, respectively. The cross-validated accuracy, sensitivity, and specificity were 76, 68, and 83%, respectively. (B) Corresponding ET cross-validated prediction plot for panel A. There were five misclassified mice. (C) oPLS-DA calibration scores plot using the 18 discriminant metabolic feature panels obtained from genetic algorithm variable selection. The model consisted of 2 LVs with 33.12 and 98.30% total captured X- and Y-block variances, respectively. The accuracy, sensitivity, and specificity were all 100%. (D) Corresponding ET cross-validated prediction plot for panel C. There were no misclassified mice.

ET DKO mice with higher cross-validated accuracy, sensitivity, and specificity. A panel of 18 metabolic features with the lowest RMSECV was selected through the genetic algorithm variable selection process. oPLS-DA modeling with this smaller panel (Figure 2C,D) resulted in 100% cross-validated accuracy, sensitivity, and specificity; therefore, no mice were misclassified. This model interpreted 33.12 and 98.30% of the X- and Y-block variances, respectively, with only two latent variables—one less than the model using all 934 metabolic features. Furthermore, the captured Y-block variance was slightly higher, thereby demonstrating that the down-selected panel of 18 features is more informative than the initial set. Of the 18 selected features, the concentration levels of 9 metabolites were found to increase and 9 metabolites were found to decrease in ET DKO mice. While only 11 of these concentration changes were univariately significant (Mann−Whitney U test, $n = 25$, $p < 0.05$; Figure 3), the covarying concentrations of all 18 metabolic features allowed us to distinguish the detected metabolomes of control and ET DKO mice in multivariate space; accordingly, they all display discriminatory power when collectively included as part of a joint panel. The concentration levels of those features that were not statistically different between ET DKO and control mice in a univariate fashion could also be a result of the relatively modest sample size used in this study.

PCA was utilized to evaluate the performance of the 18-feature discriminant panel in an unsupervised manner to further investigate these results. Scores plots were generated for both the initial set of 934 metabolic features and the 18 discriminant feature panel (Figure S2 in the Supporting Information). Using the initial set, three principal components interpreting 46.43% of

DOI: 10.1021/pr5009948
J. Proteome Res. 2015, 14, 917−927

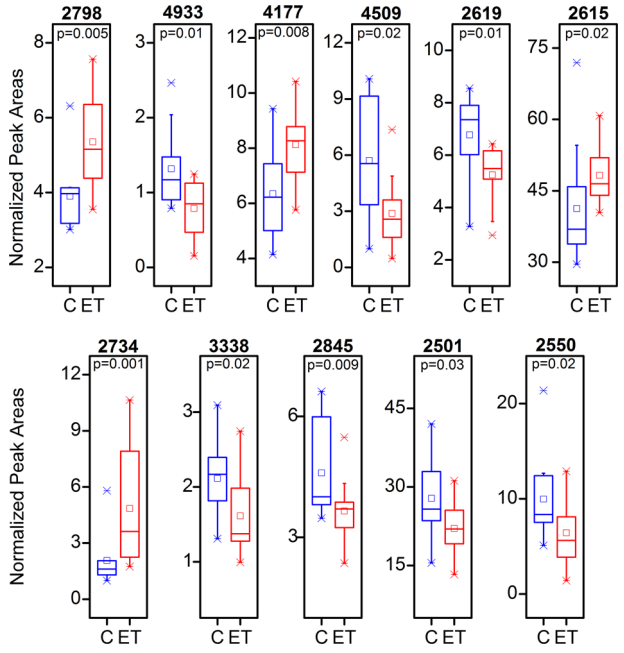

Figure 3. Discriminatory spectral features having statistically significant univariate changes between early stage tumor (ET) *Dicer-Pten* DKO mice (n = 14) and control (C) mice (n = 11). P values were calculated using the Mann−Whitney U test. Box plots with mean (square), median, upper and lower quartile, outliers, and minimum and maximum (whiskers) data values are displayed. Feature ID numbers are indicated on top of each case.

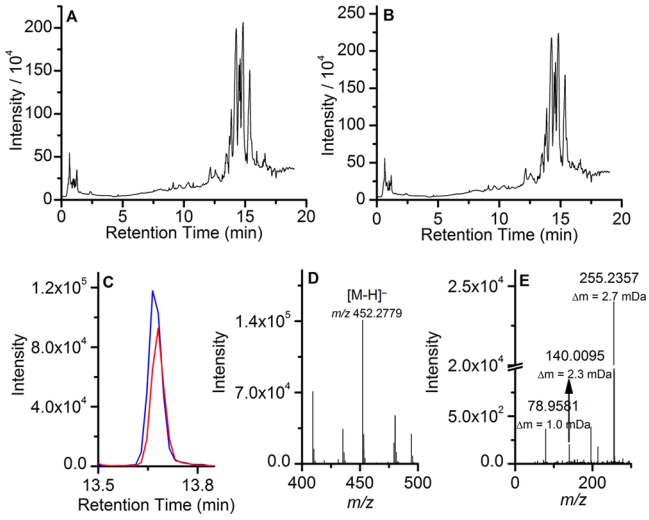

Figure 4. Typical total ion chromatograms obtained for serum samples from (A) a control mouse and (B) a *Dicer-Pten* early-stage tumor DKO mouse. (C) Extracted ion chromatogram for m/z 452.2779 ± 0.0050 generated from a control mouse sample (blue line) and a *Dicer-Pten* early-stage tumor DKO mouse (red line). These were generated from the data shown in panels A and B, respectively. (D) Mass spectrum for the discriminant metabolic feature with m/z 452.2779. (E) Tandem MS spectrum for the m/z 452.2779 precursor ion using a collision cell voltage of 30 V. The matching of the experimental tandem MS fragmentation pattern with the metabolite candidate is illustrated by the mass errors calculated as differences with the values in the MassBank database, in addition to manual fragment analysis.

the data matrix variance showed no distinct grouping of the sample classes (Figure S2A in the Supporting Information). However, better clustering was observed with the 18-feature three-principal component PCA model, which interpreted 53.49% of the variance (Figure S2B in the Supporting Information). The PCA class separation was statistically significant and occurred along the first principal component (unpaired t test, n = 25, p = 0.0055), providing further evidence of the robustness of the 18-feature discriminant panel.

Discriminant Metabolite Identification

Metabolite identification was attempted for the 18 discriminant feature subset once PCA confirmed the robustness of the oPLS-DA model. The metabolite identification procedure is illustrated in Figure 4 for feature 2501. Typical total ion UPLC−MS chromatograms for control and ET DKO mice are shown in Figure 4A,B, respectively. The apparent similarity of these chromatograms hints that subtle metabolic differences occur as HGSCs initially form and begin to proliferate and demonstrates the need for multivariate methods to extract these differences from the detected metabolomes. Highly selective accurate mass extracted ion chromatograms for each discriminant feature (Figure 4C) were generated thanks to the high resolving power of the time-of-flight mass analyzer utilized. The corresponding averaged mass spectra were used for adduct ion analysis (Figure 4D) to ensure that the correct exact mass was assigned to the spectral features of interest. The presence of multiple adducts for some features further assisted in chemical assignments. The ensuing isotopic patterns and accurate masses were used to generate lists of possible candidate elemental formulas that were searched against metabolite databases. Furthermore, UPLC−MS/MS experiments were conducted to obtain fragmentation patterns that helped confirm the metabolite identities of the 18 feature subset. Tandem MS spectra were compared with those in metabolite databases or scientific literature and manually analyzed as well (Figure 4E). Lastly, standards of the commercially available metabolites were analyzed by UPLC−MS and UPLC−MS/MS to further verify the identity of the candidates by retention time and mass spectral matching as well as eliminating nonmatches.

Eleven of the 18 metabolic features were identified by MS and MS/MS, while 4 were further confirmed chromatographically by chemical standards (Table 1). These four were ricinoleic acid (Figure 3; +0.23 fold change), bilirubin (Figure 3; −0.74 fold change), suberic acid (−0.42 fold change), and LysoPE(16:0) (Figure 3; −0.33 fold change). Extracted ion chromatograms of these 4 detected metabolites and their respective chemical standards are shown in Figure S3 in the Supporting Information. Corresponding MS and tandem MS spectra are displayed in Figures S4−S7 in the Supporting Information. Additional identified features (Table 1) include di- and triglycerides, phospholipids, bile acids, and terpenes. Four of the features in Table 1 were tentatively matched to exogenous metabolites, which have no known biofunctions, such as Peltatol A (lignan) or metabolites yet to be reported in mammals, such as (4*E*,8*E*,10*E*-*d*18:3)sphingosine (sphingoid base). These tentative metabolite identifications are listed in Table S2 in the Supporting Information, and the metabolite chemical class is still listed in Table 1 (italicized).

HGSC-Related Metabolic Alterations

The identified discriminant metabolites cover a broad range of biomolecule classes and pathways (Figure 5), many of which have been individually reported to be involved in ovarian cancer proliferation. Table 1 summarizes these findings, which are discussed based on pathway/chemical class later. Although fold

DOI: 10.1021/pr5009948
J. Proteome Res. 2015, 14, 917−927

Table 1. Confirmed and Tentative Metabolites Identified as Discriminatory between Early-Stage Tumor *Dicer-Pten* Double-Knockout Mice and Control Mice[a]

feature code	average retention time (min)[b]	average m/z[b]	fold change[c]	P value[d]	ion type	elemental formula	theoretical m/z	mass error (mDa)	tentative metabolite identification	ref
2734	11.88	294.2410	1.23	0.0011	$[M-H]^-$	$C_{18}H_{33}NO_2$	294.2439	2.9	*sphingoid base*	13,17
2798	15.53	363.2883	0.46	0.0051	$[M-H]^-$	$C_{23}H_{40}O_3$	363.2905	2.2	24-nor-5β-cholane-3α,6α,23-triol	12,18,21
									24-nor-5β-cholane-3α,7α,12α-triol	
									24-nor-5β-cholane-3α,7α,23-triol	
									24-nor-5β-cholane-3α,7β,23-triol	
									24-nor-5β-cholane-3α,12α,23-triol	
									4-hydroxy-3-(16-methylheptadecyl)-2*H*-pyran-2-one	
									2-(8-[3]-ladderane-octanyl)-*sn*-glycerol	
4177	14.81	889.7234	0.36	0.0075	$[M-H]^-$	$C_{58}H_{98}O_6$	889.7290	5.6	TG(55:7)	48
4466	13.73	625.4240	0.26	0.73	$[M-H]^-$	$C_{42}H_{58}O_4$	625.4262	2.2	*Lignan*	79
2615	**12.60**	**297.2414**	**0.23**	**0.015**	$[M-H]^-$	**$C_{18}H_{34}O_3$**	**297.2435**	**2.1**	**ricinoleic acid**	23
2489	13.37	476.2772	0.22	0.27	$[M-H]^-$	$C_{23}H_{44}NO_7P$	476.2783	1.1	LysoPE(18:2)	17,23,60
3302	11.76	163.0578	0.11	0.40	$[M-H]^-$				N/A	
3154	17.31	780.5530	0.061	0.77	$[M-H]^-$	$C_{44}H_{80}NO_8P$	780.5550	1.9	PE(39:4)	18,23,59
2537	13.33	219.1724	0.0059	0.40	$[M-H]^-$	$C_{15}H_{24}O$	219.1750	3.0	*terpene derivative*	82
4509	16.85	627.5034	−0.99	0.018	$[M-H]^-$	$C_{40}H_{68}O_5$	627.4994	4.0	DG(37:5)	49
4933	**11.49**	**583.2555**	**−0.74**	**0.011**	$[M-H]^-$	**$C_{33}H_{36}N_4O_6$**	**583.2557**	**0.7**	**bilirubin**	21
2550	14.70	711.3057	−0.63	0.025	$[M-H]^-$				N/A	
4590	1.23	345.1557	−0.52	0.29	$[M-H]^-$	$C_{16}H_{26}O_8$	345.1555	0.2	uroterpenol-*O*-glucuronide	78
						$C_{17}H_{22}N_4O_4$	345.1568	1.1	Ala-Trp-Ala[e]	18
						$C_{14}H_{26}N_4O_4S_1$	345.1602	4.5	Lys-Cys-Pro[e]	18
3226	**1.22**	**173.0810**	**−0.42**	**0.43**	$[M-H]^-$	**$C_8H_{14}O_4$**	**173.0820**	**0.9**	**suberic acid**	23,50
2619	13.43	327.2295	−0.37	0.013	$[M-H]^-$	$C_{22}H_{32}O_2$	327.2330	3.5	*fatty acid, terpene, or other phenol derivative*	23,82
2501	**13.68**	**452.2783**	**−0.33**	**0.033**	$[M-H]^-$	**$C_{21}H_{44}NO_7P$**	**452.2783**	**2.1**	**LysoPE(16:0)**	17,23,60
3338	13.33	903.6231	−0.33	0.021	$[M-H]^-$	$C_{49}H_{93}O_{12}P$	903.6332	10.1	PI(O-18:0/22:2)	23,56
									PI(P-18:0/22:1)	
									PI(O-20:0/20:2)	
									PI(P-20:0/20:1)	
2845	0.46	402.7997	−0.33	0.0090	$[M-H]^-$				N/A	

[a]Metabolites confirmed by retention time matching with commercially-available standards are highlighted in bold font. [b]These reported values were obtained after data processing with MZmine 2.0 software, which generates average values calculated using all samples. [c]Fold change was calculated as the base 2 logarithm of the average peak area ratios for ET DKO mouse samples and control samples. [d]P values calculated using Mann−Whitney U test. [e]Other polypeptide isomers are not listed; tandem MS data could not be acquired to confirm true isomer identity because their ion abundances were not high enough for quadrupole selection.

changes are reported in this discussion, the only statistically significant metabolite fold changes were those shown in Figure 3.

Fatty Acids and Derivatives

The development of hormone-related cancers, such as ovarian cancer, may be influenced by fatty acids.[39] Fatty acids are involved in tumor cell signaling and growth and are also used for energy expenditure, bulk membrane synthesis, and membrane-targeted protein modifications.[40,41] Thus, it is not surprising that changes in fatty acid concentrations aid in detecting the early stages of HGSC development in the DKO mouse model. Five features in our discriminant subset were tentatively identified as fatty acids or their derivatives (Table 1; Figure 5): TG(55:7), ricinoleic acid, DG(37:5), suberic acid, and an unidentified possible fatty acid ($C_{22}H_{32}O_2$).

Estrogens, which play a major role in ovarian cancer proliferation,[42] have been linked with increased hepatic triglyceride production and secretion into blood in mice,[43] chickens,[44,45] and humans.[46,47] Accordingly, increased blood serum triglyceride concentrations have been linked to gynecological (ovarian, endometrial, cervical) cancer risk,[48] in agreement with our finding in ET DKO mice (Table 1; Figure 3; fold change: +0.36). Gercel-Taylor et al. found increased diglyceride levels in the ascites of late-stage ovarian cancer patients,[49] which is opposite to the decrease found in this study in the serum from mice with early stage tumors (Table 1; Figure 3; fold change: −0.99). Because diglycerides are precursors to triglycerides, decreased diglyceride levels could be the result of increased triglyceride synthesis in the ET DKO mice, further demonstrating that HGSCs impact energy storage and generation. As a note, the identified odd-chain di- and triglycerides could also result

DOI: 10.1021/pr5009948
J. Proteome Res. 2015, 14, 917−927

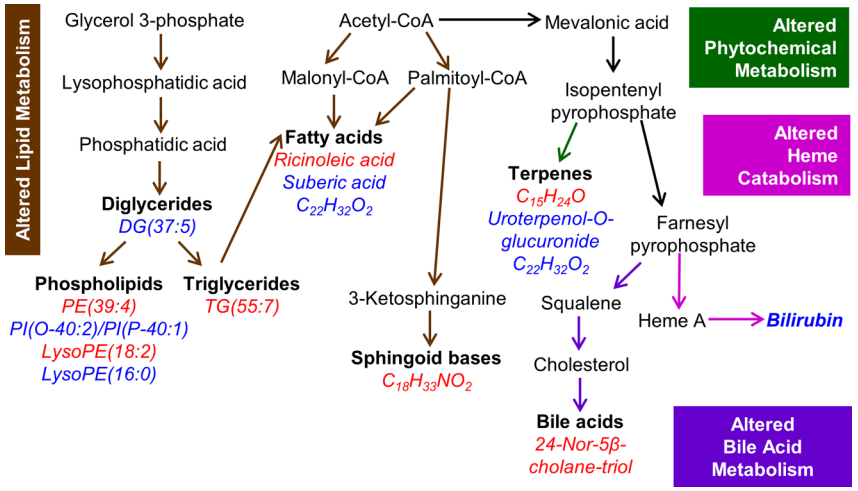

Figure 5. Overview of key altered metabolic/catabolic pathways observed in early stage tumor (ET) *Dicer-Pten* DKO mice. Arrows are colored based on their corresponding altered pathways and represent both direct and indirect relationships between metabolites/metabolite classes. Metabolites from the 18 discriminant feature subset are italicized, and their corresponding metabolite class is in bold. Metabolites in red text have increased levels in ET DKO mice, while those in blue text have decreased levels in ET DKO mice. Metabolite relationships were derived from Kyoto Encyclopedia of Genes and Genomes,[83] MetaCyc,[84] and existing scientific literature.

from dietary intake, thus hinting that fatty acid catabolism could be occurring at a decreased rate in ET DKO mice.

Suberic acid, a metabolic breakdown product of oleic acid, had decreased serum levels (Table 1; fold change: −0.42) in ET DKO mice. Menendez et al. found that oleic acid suppresses the transcriptional activity of the Her-2/*neu* oncogene in the SK-OV3 ovarian cancer cell line by up-regulating polyomavirus enhancer activator 3 (PEA3), a Her-2/*neu* promoter transcriptional repressor.[50] The detected decrease in suberic acid may thus be indirectly connected to the anticancer properties offered by oleic acid. Additionally, conjugated linoleic acid has been shown to suppress epidermal and mammary carcinogenesis in mice.[51,52] The detected increase in serum levels of ricinoleic acid (Table 1; Figure 3; fold change: +0.23) in ET DKO mice could thus be related to its increased production for further conversion into other fatty acids such as conjugated linoleic acid, as reported for bacteria.[53,54] In a metabolomics study, Denkert et al. detected decreased levels of free fatty acids (nonadecanoic acid, stearic acid, heptadecanoic acid) in invasive ovarian carcinoma tumors compared with borderline ovarian tumors.[23] Correspondingly, the serum levels of the unidentified possible $C_{22}H_{32}O_2$ fatty acid (Table 1; Figure 3; fold change: −0.37) were also decreased in the ET DKO mice.

Phospholipids

Cancer cells need a continuous supply of phospholipids for generation and maintenance of membrane integrity as well as for protein modifications.[55] Four features in our discriminant subset were tentatively identified as phospholipids (Table 1; Figure 5): LysoPE (18:2), PE(39:4), LysoPE(16:0), and $C_{49}H_{93}O_{12}P$ [PI(O-18:0/22:2), PI(P-18:0/22:1), PI(O-20:0/20:2), or PI(P-20:0/20:1)]. The detected changes in phospholipids suggest membrane degradation or morphological changes in HGSC-affected cells because these lipids play a role in maintaining cellular membrane integrity. However, the interpretation of both increased and decreased levels is not straightforward and could be the result of membrane instability and the subsequent attempt of cancer cells to repair them.

The PIK3CA oncogene, whose encoded protein phosphorylates phosphatidylinositols, as well as increased PI3-kinase activity have been implicated in ovarian carcinogenesis.[56] Links between PI3-kinase activation and increased cell survival due to the suppression of apoptosis have also been established.[57,58] Moreover, increased PI3-kinase activity may aid in cancer proliferation by increasing cellular motility.[56] The observed PI ($C_{49}H_{93}O_{12}P$) decrease (Table 1; Figure 3; fold change: −0.33) in ET DKO mice could thus be attributed to increased PI3-kinase activity. As the conditional deletion of *Pten* from ET DKO mice activates the PI3-kinase signaling pathway, increased PI3-kinase activity could also be an artifact of the genetic manipulation of the mice.[30]

Serum levels of PE(39:4) (Table 1; fold change: +0.061) were increased in ET DKO mice. Previous work by our group also found that a collection of phosphatidylethanolamines aided in combined early- and late-stage HGSC detection in human subjects.[18] Moreover, choline kinase, an enzyme needed for the synthesis of phosphatidylethanolamines and phosphatidylcholines, has been shown to be increased in the EOC cell lines SK-OV3 and OVCAR-3.[59] Lysophosphatidylethanolamine has been shown to increase intracellular calcium concentrations and stimulate an unknown membrane receptor, causing chemotactic migration and cell invasion in the SK-OV3 ovarian cancer cell line.[60] Although there are no definite conclusions to be drawn from the increased (Table 1; fold change: +0.22) and decreased (Table 1; Figure 3: fold change: −0.33) levels of lysophosphatidylethanolamines detected in ET DKO mice, these changes could be related to the initiation of migration and invasion of HGSC to neighboring tissue during proliferation. Moreover, LysoPE(18:2) has recently been shown to aid in the detection of prostate cancer, another hormone-related cancer.[61]

Sphingoid Bases

Sphingoid bases, particularly sphingosine, have been long implicated in playing a role in cancer biology. One of the features in the discriminating subset was an unidentified $C_{18}H_{33}NO_2$ sphingoid base (Table 1; Figure 5). Sphingosine facilitates and triggers apoptosis, while sphingosine 1-phosphate promotes cellular survival/profileration in response to apoptotic stress.[62] Illuzzi et al. found that inhibiting sphingosine kinase, thereby suppressing the production of sphingosine 1-phosphate

DOI: 10.1021/pr5009948
J. Proteome Res. 2015, 14, 917−927

from sphingosine, reduced cell proliferation in ovarian cancer cell lines.[63] Research by Hong et al. suggested that sphingosine 1-phosphate is a vital component of cellular growth and adhesion modulation for ovarian cancer cell lines HEY and OCC1.[64] Increased levels of the $C_{18}H_{33}NO_2$ sphingoid base in ET DKO mice (Table 1; Figure 3; fold change: +1.23) therefore hint at a "biochemical fight response" toward the developing carcinoma. Supporting this hypothesis, Fan et al. detected increased plasma levels of the sphingolipids phytosphingosine, ganglioside, and ceramides in a cohort combining early- and late-stage EOC patients that were compared with healthy controls.[17] Additionally, Chen et al. observed an increase in phytosphingosine in the urine of a combined early- and late-stage EOC patient cohort.[13]

Bile Acids, Alcohols, and Derivatives

Bile acids cause apoptosis as well as oxidative stress in cells, resulting in the generation of reactive oxygen species (ROS) that subsequently damage DNA. Recurring DNA damage can increase mutation rates of onco- and tumor suppressor genes. Therefore, cells exposed to bile acids can proliferate, leading to carcinogenesis.[65] Two features in our discriminant feature subset were tentatively identified as bile acids and related substances (Table 1; Figure 5): 24-nor-5β-cholane-triol and bilirubin. Serum levels of 24-nor-5β-cholane-triol were found to be increased (Table 1; Figure 3; fold change: +0.46) in ET DKO mice. It is plausible that ROS generation by 24-nor-5β-cholane-triol aided in the development of ovarian carcinoma in ET DKO mice. In agreement with these findings, Chen et al. identified 27-nor-5β-cholestane-3,7,12,24,25 pentol glucuronide (CPG) as a serum biomarker for combined early- and late-stage EOC, which was also accompanied by increased levels of glycocholic acid.[21] Also supporting this finding is previous work by our group, showing that bile acids, specifically isomers of 5β-chol-9(11)-en-24-oic acid, can aid in the detection of human HGSC.[18]

Although bilirubin is not a bile acid, it is a component of bile and the end product of heme catabolism. Furthermore, increased bilirubin has been associated with low cancer mortality.[66] Bilirubin acts as an endogenous antioxidant that reduces oxidative stress damage by scavenging peroxyl[67] and hydroxyl radicals.[68] Moreover, mutations in the tumor suppressor gene *p53* can be caused by ROS,[69] and *p53* mutations are found in many cancers, including ovarian cancer.[70,71] Lowered concentration levels of bilirubin, as detected in the ET DKO mice (Table 1; Figure 3; fold change: −0.74), possibly imply diminished protection against ROS, thus leading to carcinogenesis. Supporting this hypothesis, Chen et al. tentatively detected decreased levels of bilirubin in the serum of both early- and late-stage EOC patients and increased levels of bilirubin mono- and diglucuronic acids.[21]

Peptides

One member of the discriminant feature subset was tentatively identified as a tripeptide isomer of Ala-Trp-Ala or Lys-Cys-Pro (Table 1). Tandem MS data could not be acquired to confirm the tripeptide sequence as the precursor ion abundances were not sufficiently high. Blood serum levels of these peptides were decreased in ET DKO mice (Table 1; fold change: −0.52). Previous work by our group has also found that tripeptides, specifically Gln-His-Ala or its isomers, aided in human HGSC detection.[18] However, a survey of the literature revealed no mechanism by which small circulating peptides could play a biological role in ovarian cancer. Some proteases have been reported to be overexpressed in ovarian carcinoma,[72−74] but we would expect liberated peptides to have an increased concentration in ET DKO mice if their presence resulted from increased protease activity.

Phytochemicals - Terpenes

Three features in our discriminant subset were tentatively identified as terpenes (Table 1; Figure 5): a $C_{15}H_{24}O$ terpene derivative, uroterpenol-*O*-glucuronide, and an unidentified terpene ($C_{22}H_{32}O_2$). Many terpenes enter metabolic networks from food sources. Although both ET DKO and control mice were fed the same diet, it is plausible that the presence of HGSC in ET DKO mice altered the metabolism of dietary metabolites. Uroterpenol is a metabolic product of limonene, a terpene component of citrus fruits, vegetables, herbs, and spices, and has been shown to lengthen tumor latency and decrease tumor yield in mice with mammary cancer.[77] Interestingly, uroterpenol-*O*-glucuronide has been found to have urinary excretion patterns resembling those of estriol, pregnanediol, and pregnanetriol, and increased excretions have been associated with increased placental, ovarian, or adrenal activity.[78] The decreased serum levels of uroterpenol-*O*-glucuronide observed in ET DKO mice (Table 1; fold change: −0.52) might thus relate to increased ovarian activity or to decreased serum uroterpenol concentrations.

Phytochemicals - Lignans

One feature in our discriminant subset was an unidentified $C_{42}H_{58}O_4$ lignan. Lignans are phytoestrogens that are abundant in diets of people living in regions of low cancer incidence.[79] An increased dietary lignan intake, measured by urinary excretion, has been correlated with reduced breast cancer risk.[80] Ovarian cancer tumors contain type II estrogen binding sites,[81] and it has been suggested that lignans inhibit cancer cell growth by competing with estradiol for type II estrogen binding sites.[79] Because there was a detected increase in the unidentified $C_{42}H_{58}O_4$ lignan (Table 1; fold change: +0.26) in the serum of ET DKO mice, it is possible that binding of lignans to type II estrogen sites was somehow decreased, thereby not aiding in the inhibition of HGSC proliferation.

CONCLUSIONS

Early-stage HGSC was successfully detected in a *Dicer-Pten* DKO mice model utilizing UPLC−MS untargeted metabolic profiling. After down-selection of spectral features with maximum discriminatory power, 18 metabolites differentiated DKO mice with early stage tumors from control mice with 100% accuracy, sensitivity, and specificity. Altered metabolic pathways included those of fatty acids, bile acids and alcohols, glycerophospholipids, peptides, and phytochemicals. These alterations impact cellular energy storage and membrane stability as well as defenses against oxidative stress. This work is the first step toward understanding the underlying metabolic changes resulting from the progression of early HGSCs originating in the fallopian tube. Exploration of the overlap between DKO mice and humans in early stages of HGSC development will be pursued in the future.

ASSOCIATED CONTENT

Supporting Information

Data set S1: Complete metabolic feature data set. Table S1: Early-stage tumor *Dicer-Pten* double-knockout mice and control mice characteristics. Table S2: Exogenous metabolites or metabolites not reported in mammals identified as discriminatory between early-stage tumor *Dicer-Pten* DKO and control mice. Figure S1: Proof-of-concept experiment PCA scores plot of

DOI: 10.1021/pr5009948
J. Proteome Res. 2015, 14, 917−927

early-stage tumor *Dicer-Pten* DKO, late-stage tumor *Dicer-Pten* DKO mice, and control mice. Figure S2: PCA of early-stage tumor *Dicer-Pten* DKO and control mice. Figure S3: Extracted ion chromatograms from chemical standard metabolite identification experiments. Figures S4−S7: Full-scan MS spectrum and tandem MS fragmentation spectra from chemical standard metabolite identification experiments. This material is available free of charge via the Internet at http://pubs.acs.org.

AUTHOR INFORMATION

Corresponding Author

*E-mail: facundo.fernandez@chemistry.gatech.edu. Tel: 404 385 4432. Fax: 404 385 3399.

Present Address

◆M.E.M.: Centro de Investigaciones en Bionanociencias (CIBION), Consejo Nacional de Investigaciones Científicas y Técnicas (CONICET), Godoy Cruz 2390, C1425FQD, CABA, Argentina.

Notes

The authors declare no competing financial interest.

ACKNOWLEDGMENTS

We acknowledge support from an Ovarian Cancer Research Fund (OCRF) Program Project Development grant and the Marsha Rivkin Foundation.

REFERENCES

(1) Siegel, R.; Naishadham, D.; Jemal, A. Cancer statistics, 2013. *Ca-Cancer J. Clin.* **2013**, *63* (1), 11−30.
(2) Cho, K. R.; Shih, I. Ovarian cancer. *Annu. Rev. Pathol.* **2009**, *4*, 287−313.
(3) Bast, R. C., Jr.; Hennessy, B.; Mills, G. B. The biology of ovarian cancer: New opportunities for translation. *Nat. Rev. Cancer* **2009**, *9* (6), 415−428.
(4) TCGA. Integrated genomic analyses of ovarian carcinoma. *Nature* **2011**, *474* (7353), 609−615.
(5) Bhoola, S.; Hoskins, W. J. Diagnosis and management of epithelial ovarian cancer. *Obstet. Gynecol.* **2006**, *107* (6), 1399−1410.
(6) Seidman, J. D.; Zhao, P.; Yemelyanova, A. "Primary peritoneal" high-grade serous carcinoma is very likely metastatic from serous tubal intraepithelial carcinoma: Assessing the new paradigm of ovarian and pelvic serous carcinogenesis and its implications for screening for ovarian cancer. *Gynecol. Oncol.* **2011**, *120* (3), 470−473.
(7) Williams, T. I.; Toups, K. L.; Saggese, D. A.; Kalli, K. R.; Cliby, W. A.; Muddiman, D. C. Epithelial ovarian cancer: Disease etiology, treatment, detection, and investigational gene, metabolite, and protein biomarkers. *J. Proteome Res.* **2007**, *6* (8), 2936−2962.
(8) Bristow, R. E.; Hodeib, M.; Smith, A.; Chan, D. W.; Zhang, Z.; Fung, E. T.; Tewari, K. S.; Munroe, D. G.; Ueland, F. R. Impact of a multivariate index assay on referral patterns for surgical management of an adnexal mass. *Am. J. Obstet. Gynecol.* **2013**, *209* (6), 581.e1−581.e8.
(9) Ueland, F. R.; Desimone, C. P.; Seamon, L. G.; Miller, R. A.; Goodrich, S.; Podzielinski, I.; Sokoll, L.; Smith, A.; van Nagell, J. R.; Zhang, Z. Effectiveness of a multivariate index assay in the preoperative assessment of ovarian tumors. *Obstet. Gynecol.* **2011**, *117* (6), 1289−1297.
(10) Zhang, Z. An in vitro diagnostic multivariate index assay (IVDMIA) for ovarian cancer: Harvesting the power of multiple biomarkers. *Rev. Obstet. Gynecol.* **2012**, *5* (1), 35−41.
(11) American College of Obstetricians and Gynecologists, Committee Opinion 477. The role of the obstetrician-gynecologist in the early detection of epithelial ovarian cancer. *Obstet. Gynecol.* **2011**, *117* (3), 742−746.
(12) Zhang, T.; Wu, X. Y.; Ke, C. F.; Yin, M. Z.; Li, Z. Z.; Fan, L. J.; Zhang, W.; Zhang, H. Y.; Zhao, F. L.; Zhou, X. H.; Lou, G.; Li, K. Identification of potential biomarkers for ovarian cancer by urinary metabolomic profiling. *J. Proteome Res.* **2013**, *12* (1), 505−512.
(13) Chen, J.; Zhou, L. N.; Zhang, X. Y.; Lu, X.; Cao, R.; Xu, C. J.; Xu, G. W. Urinary hydrophilic and hydrophobic metabolic profiling based on liquid chromatography-mass spectrometry methods: Differential metabolite discovery specific to ovarian cancer. *Electrophoresis* **2012**, *33* (22), 3361−3369.
(14) Slupsky, C. M.; Steed, H.; Wells, T. H.; Dabbs, K.; Schepansky, A.; Capstick, V.; Faught, W.; Sawyer, M. B. Urine metabolite analysis offers potential early diagnosis of ovarian and breast cancers. *Clin. Cancer Res.* **2010**, *16* (23), 5835−5841.
(15) Woo, H. M.; Kim, K. M.; Choi, M. H.; Jung, B. H.; Lee, J.; Kong, G.; Nam, S. J.; Kim, S.; Bai, S. W.; Chung, B. C. Mass spectrometry based metabolomic approaches in urinary biomarker study of women's cancers. *Clin. Chim. Acta* **2009**, *400* (1), 63−69.
(16) Zhang, T.; Wu, X. Y.; Yin, M. Z.; Fan, L. J.; Zhang, H. Y.; Zhao, F. L.; Zhang, W.; Ke, C. F.; Zhang, G. M.; Hou, Y.; Zhou, X. H.; Lou, G.; Li, K. Discrimination between malignant and benign ovarian tumors by plasma metabolomic profiling using ultra performance liquid chromatography/mass spectrometry. *Clin. Chim. Acta* **2012**, *413* (9−10), 861−868.
(17) Fan, L. J.; Zhang, W.; Yin, M. Z.; Zhang, T.; Wu, X. Y.; Zhang, H. Y.; Sun, M.; Li, Z. Z.; Hou, Y.; Zhou, X. H.; Lou, G.; Li, K. Identification of metabolic biomarkers to diagnose epithelial ovarian cancer using a UPLC/QTOF/MS platform. *Acta Oncol.* **2012**, *51* (4), 473−479.
(18) Guan, W.; Zhou, M.; Hampton, C.; Benigno, B.; Walker, L. D.; Gray, A.; McDonald, J.; Fernandez, F. Ovarian cancer detection from metabolomic liquid chromatography/mass spectrometry data by support vector machines. *BMC Bioinf.* **2009**, *10* (1), 259.
(19) Odunsi, K.; Wollman, R. M.; Ambrosone, C. B.; Hutson, A.; McCann, S. E.; Tammela, J.; Geisler, J. P.; Miller, G.; Sellers, T.; Cliby, W.; Qian, F.; Keitz, B.; Intengan, M.; Lele, S.; Alderfer, J. L. Detection of epithelial ovarian cancer using ^{1}H-NMR-based metabonomics. *Int. J. Cancer* **2005**, *113* (5), 782−788.
(20) Garcia, E.; Andrews, C.; Hua, J.; Kim, H. L.; Sukumaran, D. K.; Szyperski, T.; Odunsi, K. Diagnosis of early stage ovarian cancer by ^{1}H NMR metabonomics of serum explored by use of a microflow NMR probe. *J. Proteome Res.* **2011**, *10* (4), 1765−1771.
(21) Chen, J.; Zhang, X. Y.; Cao, R.; Lu, X.; Zhao, S. M.; Fekete, A.; Huang, Q.; Schmitt-Kopplin, P.; Wang, Y. S.; Xu, Z. L.; Wan, X. P.; Wu, X. H.; Zhao, N. Q.; Xu, C. J.; Xu, G. W. Serum 27-nor-5 beta-Cholestane-3,7,12,24,25 Pentol Glucuronide discovered by metabolomics as potential diagnostic biomarker for epithelium ovarian cancer. *J. Proteome Res.* **2011**, *10* (5), 2625−2632.
(22) Zhou, M. S.; Guan, W.; Walker, L. D.; Mezencev, R.; Benigno, B. B.; Gray, A.; Fernandez, F. M.; McDonald, J. F. Rapid mass spectrometric metabolic profiling of blood sera detects ovarian cancer with high accuracy. *Cancer Epidemiol., Biomarkers Prev.* **2010**, *19* (9), 2262−2271.
(23) Denkert, C.; Budczies, J.; Kind, T.; Weichert, W.; Tablack, P.; Sehouli, J.; Niesporek, S.; Konsgen, D.; Dietel, M.; Fiehn, O. Mass spectrometry-based metabolic profiling reveals different metabolite patterns in invasive ovarian carcinomas and ovarian borderline tumors. *Cancer Res.* **2006**, *66* (22), 10795−10804.
(24) Ben Sellem, D.; Elbayed, K.; Neuville, A.; Moussallieh, F.-M.; Lang-Averous, G.; Piotto, M.; Bellocq, J.-P.; Namer, I. Metabolomic characterization of ovarian epithelial carcinomas by HRMAS-NMR spectroscopy. *J. Oncol.* **2011**, *2011*, 174019.
(25) Fong, M. Y.; McDunn, J.; Kakar, S. S. Identification of metabolites in the normal ovary and their transformation in primary and metastatic ovarian cancer. *PloS One* **2011**, *6* (5), e19963.
(26) Moyer, V. A. Screening for ovarian cancer: U.S. preventive services task force reaffirmation recommendation statement. *Ann. Int. Med.* **2012**, *157* (12), 900−904.
(27) Piek, J. M.; van Diest, P. J.; Zweemer, R. P.; Jansen, J. W.; Poort-Keesom, R. J.; Menko, F. H.; Gille, J. J.; Jongsma, A. P.; Pals, G.; Kenemans, P.; Verheijen, R. H. Dysplastic changes in prophylactically removed Fallopian tubes of women predisposed to developing ovarian cancer. *J. Pathol.* **2001**, *195* (4), 451−456.

DOI: 10.1021/pr5009948
J. Proteome Res. 2015, 14, 917−927

(28) Crum, C. P.; Drapkin, R.; Kindelberger, D.; Medeiros, F.; Miron, A.; Lee, Y. Lessons from BRCA: The tubal fimbria emerges as an origin for pelvic serous cancer. *Clin. Med. Res.* **2007**, *5* (1), 35−44.
(29) Kurman, R. J.; Shih, I. The origin and pathogenesis of epithelial ovarian cancer: A proposed unifying theory. *Am. J. Surg. Pathol.* **2010**, *34* (3), 433−443.
(30) Kim, J.; Coffey, D. M.; Creighton, C. J.; Yu, Z.; Hawkins, S. M.; Matzuk, M. M. High-grade serous ovarian cancer arises from fallopian tube in a mouse model. *Proc. Natl. Acad. Sci. U.S.A.* **2012**, *109* (10), 3921−3926.
(31) Trygg, J.; Wold, S. Orthogonal projections to latent structures (O-PLS). *J. Chemom.* **2002**, *16* (3), 119−128.
(32) Pluskal, T.; Castillo, S.; Villar-Briones, A.; Orešič, M. MZmine 2: Modular framework for processing, visualizing, and analyzing mass spectrometry-based molecular profile data. *BMC Bioinf.* **2010**, *11* (1), 395.
(33) Smith, C. A.; O'Maille, G.; Want, E. J.; Qin, C.; Trauger, S. A.; Brandon, T. R.; Custodio, D. E.; Abagyan, R.; Siuzdak, G. METLIN: A metabolite mass spectral database. *Ther. Drug Monit.* **2005**, *27* (6), 747−751.
(34) Sud, M.; Fahy, E.; Cotter, D.; Brown, A.; Dennis, E. A.; Glass, C. K.; Merrill, A. H.; Murphy, R. C.; Raetz, C. R. H.; Russell, D. W.; Subramaniam, S. LMSD: LIPID MAPS structure database. *Nucleic Acids Res.* **2007**, *35* (suppl 1), D527−D532.
(35) Wishart, D. S.; Tzur, D.; Knox, C.; Eisner, R.; Guo, A. C.; Young, N.; Cheng, D.; Jewell, K.; Arndt, D.; Sawhney, S. HMDB: The human metabolome database. *Nucleic Acids Res.* **2007**, *35* (suppl 1), D521−D526.
(36) Zhou, B.; Wang, J.; Ressom, H. W. MetaboSearch: Tool for mass-based metabolite identification using multiple databases. *PloS One* **2012**, *7* (6), e40096.
(37) Douglas, D. J.; Konenkov, N. V. Ion source emittance influence on the transmission of a quadrupole operated in the second stability region. *J. Am. Soc. Mass Spectrom.* **1998**, *9* (10), 1074−1080.
(38) Horai, H.; Arita, M.; Kanaya, S.; Nihei, Y.; Ikeda, T.; Suwa, K.; Ojima, Y.; Tanaka, K.; Tanaka, S.; Aoshima, K. MassBank: A public repository for sharing mass spectral data for life sciences. *J. Mass Spectrom.* **2010**, *45* (7), 703−714.
(39) Risch, H. A.; Jain, M.; Marrett, L. D.; Howe, G. R. Dietary fat intake and risk of epithelial ovarian cancer. *J. Natl. Cancer Inst.* **1994**, *86* (18), 1409−1415.
(40) DeBerardinis, R. J.; Sayed, N.; Ditsworth, D.; Thompson, C. B. Brick by brick: Metabolism and tumor cell growth. *Curr. Opin. Genet. Dev.* **2008**, *18* (1), 54−61.
(41) Argiles, J. M.; Alvarez, B.; López-Soriano, F. J. The metabolic basis of cancer cachexia. *Med. Res. Rev.* **1997**, *17* (5), 477−498.
(42) O'Donnell, A. J. M.; Macleod, K. G.; Burns, D. J.; Smyth, J. F.; Langdon, S. P. Estrogen receptor-α mediates gene expression changes and growth response in ovarian cancer cells exposed to estrogen. *Endocr-Relat. Cancer* **2005**, *12* (4), 851−866.
(43) Kim, H.-J.; Kalkhoff, R. Sex steroid influence on triglyceride metabolism. *J. Clin. Invest.* **1975**, *56* (4), 888.
(44) Park, J. R.; Cho, B. S. Changes in plasma lipids, lipoproteins, triglyceride secretion and removal in chicks with estrogen implants. *Lipids* **1988**, *23* (4), 327−333.
(45) Kudzma, D. J.; Hegstad, P. M.; Stoll, R. E. The chick as a laboratory model for the study of estrogen-induced hyperlipidemia. *Metabolism* **1973**, *22* (3), 423−434.
(46) Hazzard, W. R.; Spiger, M. J.; Bagdade, J. D.; Bierman, E. L. Studies on the mechanism of increased plasma triglyceride levels induced by oral contraceptives. *New Engl. J. Med.* **1969**, *280* (9), 471−474.
(47) O'Brien, T.; Nguyen, T. T. Lipids and Lipoproteins in Women. *Mayo Clin. Proc.* **1997**, *72* (3), 235−244.
(48) Ulmer, H.; Borena, W.; Rapp, K.; Klenk, J.; Strasak, A.; Diem, G.; Concin, H.; Nagel, G. Serum triglyceride concentrations and cancer risk in a large cohort study in Austria. *Br. J. Cancer* **2009**, *101* (7), 1202−1206.
(49) Gercel-Taylor, C.; Doering, D. L.; Kraemer, F. B.; Taylor, D. D. Aberrations in normal systemic lipid metabolism in ovarian cancer patients. *Gynecol. Oncol.* **1996**, *60* (1), 35−41.
(50) Menendez, J. A.; Papadimitropoulou, A.; Vellon, L.; Lupu, R. A genomic explanation connecting "Mediterranean diet", olive oil and cancer: Oleic acid, the main monounsaturated fatty acid of olive oil, induces formation of inhibitory "PEA3 transcription factor-PEA3 DNA binding site" complexes at the Her-2/ *neu* (*erb*B-2) oncogene promoter in breast, ovarian and stomach cancer cells. *Eur. J. Cancer* **2006**, *42* (15), 2425−2432.
(51) Ha, Y.; Grimm, N.; Pariza, M. Anticarcinogens from fried ground beef: Heat-altered derivatives of linoleic acid. *Carcinogenesis* **1987**, *8* (12), 1881−1887.
(52) Ip, C.; Chin, S. F.; Scimeca, J. A.; Pariza, M. W. Mammary cancer prevention by conjugated dienoic derivative of linoleic acid. *Cancer Res.* **1991**, *51* (22), 6118−6124.
(53) Ando, A.; Ogawa, J.; Kishino, S.; Shimizu, S. CLA production from ricinoleic acid by lactic acid bacteria. *J. Am. Oil Chem. Soc.* **2003**, *80* (9), 889−894.
(54) Ando, A.; Ogawa, J.; Kishino, S.; Shimizu, S. Conjugated linoleic acid production from castor oil by *Lactobacillus plantarum* JCM 1551. *Enzyme Microb. Technol.* **2004**, *35* (1), 40−45.
(55) Rysman, E.; Brusselmans, K.; Scheys, K.; Timmermans, L.; Derua, R.; Munck, S.; Van Veldhoven, P. P.; Waltregny, D.; Daniëls, V. W.; Machiels, J. De novo lipogenesis protects cancer cells from free radicals and chemotherapeutics by promoting membrane lipid saturation. *Cancer Res.* **2010**, *70* (20), 8117−8126.
(56) Shayesteh, L.; Lu, Y.; Kuo, W.-L.; Baldocchi, R.; Godfrey, T.; Collins, C.; Pinkel, D.; Powell, B.; Mills, G. B.; Gray, J. W. PIK3CA is implicated as an oncogene in ovarian cancer. *Nat. Genet.* **1999**, *21* (1), 99−102.
(57) Kennedy, S. G.; Wagner, A. J.; Conzen, S. D.; Jordan, J.; Bellacosa, A.; Tsichlis, P. N.; Hay, N. The PI 3-kinase/Akt signaling pathway delivers an anti-apoptotic signal. *Genes Dev.* **1997**, *11* (6), 701−713.
(58) Kulik, G.; Klippel, A.; Weber, M. J. Antiapoptotic signalling by the insulin-like growth factor I receptor, phosphatidylinositol 3-kinase, and Akt. *Mol. Cell. Biol.* **1997**, *17* (3), 1595−1606.
(59) Iorio, E.; Ricci, A.; Bagnoli, M.; Pisanu, M. E.; Castellano, G.; Di Vito, M.; Venturini, E.; Glunde, K.; Bhujwalla, Z. M.; Mezzanzanica, D. Activation of phosphatidylcholine cycle enzymes in human epithelial ovarian cancer cells. *Cancer Res.* **2010**, *70* (5), 2126−2135.
(60) Park, K. S.; Lee, H. Y.; Lee, S. Y.; Kim, M.-K.; Kim, S. D.; Kim, J. M.; Yun, J.; Im, D.-S.; Bae, Y.-S. Lysophosphatidylethanolamine stimulates chemotactic migration and cellular invasion in SK-OV3 human ovarian cancer cells: Involvement of pertussis toxin-sensitive G-protein coupled receptor. *FEBS Lett.* **2007**, *581* (23), 4411−4416.
(61) Zang, X.; Jones, C. M.; Long, T. Q.; Monge, M. E.; Zhou, M.; Walker, L. D.; Mezencev, R.; Gray, A.; McDonald, J. F.; Fernandez, F. M. Feasibility of detecting prostate cancer by ultra performance liquid chromatography−mass spectrometry serum metabolomics. *J. Proteome Res.* **2014**, *13* (7), 3444−3454.
(62) Cuvillier, O. Sphingosine kinase-1−a potential therapeutic target in cancer. *Anti-Cancer Drugs* **2007**, *18* (2), 105−110.
(63) Illuzzi, G.; Bernacchioni, C.; Aureli, M.; Prioni, S.; Frera, G.; Donati, C.; Valsecchi, M.; Chigorno, V.; Bruni, P.; Sonnino, S. Sphingosine kinase mediates resistance to the synthetic retinoid N-(4-hydroxyphenyl) retinamide in human ovarian cancer cells. *J. Biol. Chem.* **2010**, *285* (24), 18594−18602.
(64) Hong, G.; Baudhuin, L. M.; Xu, Y. Sphingosine-1-phosphate modulates growth and adhesion of ovarian cancer cells. *FEBS Lett.* **1999**, *460* (3), 513−518.
(65) Bernstein, H.; Bernstein, C.; Payne, C.; Dvorakova, K.; Garewal, H. Bile acids as carcinogens in human gastrointestinal cancers. *Mutat. Res., Rev. Mutat. Res.* **2005**, *589* (1), 47−65.
(66) Temme, E. H.; Zhang, J.; Schouten, E. G.; Kesteloot, H. Serum bilirubin and 10-year mortality risk in a Belgian population. *Cancer, Causes Control, Pap. Symp.* **2001**, *12* (10), 887−894.

DOI: 10.1021/pr5009948
J. Proteome Res. 2015, 14, 917−927

(67) Stocker, R.; Yamamoto, Y.; McDonagh, A. F.; Glazer, A. N.; Ames, B. N. Bilirubin is an antioxidant of possible physiological importance. *Science* **1987**, *235* (4792), 1043−1046.
(68) Neužil, J.; Stocker, R. Bilirubin attenuates radical-mediated damage to serum albumin. *FEBS Lett.* **1993**, *331* (3), 281−284.
(69) Hussain, S. P.; Aguilar, F.; Amstad, P.; Cerutti, P. Oxy-radical induced mutagenesis of hotspot codons 248 and 249 of the human p53 gene. *Oncogene* **1994**, *9* (8), 2277−2281.
(70) Marks, J.; Davidoff, A.; Kerns, B.; Humphrey, P.; Pence, J.; Dodge, R.; Clarke-Pearson, D.; Iglehart, J.; Bast, R.; Berchuck, A. Over-expression and mutation of p53 in epithelial ovarian cancer. *Cancer Res.* **1991**, *51* (11), 2979−2984.
(71) Kupryjańczyk, J.; Thor, A. D.; Beauchamp, R.; Merritt, V.; Edgerton, S. M.; Bell, D. A.; Yandell, D. W. p53 gene mutations and protein accumulation in human ovarian cancer. *Proc. Natl. Acad. Sci. U.S.A.* **1993**, *90* (11), 4961−4965.
(72) Diamandis, E. P.; Yousef, G. M.; Soosaipillai, A. R.; Bunting, P. Human kallikrein 6 (zyme/protease M/neurosin): A new serum biomarker of ovarian carcinoma. *Clin. Biochem.* **2000**, *33* (7), 579−583.
(73) Tanimoto, H.; Yan, Y.; Clarke, J.; Korourian, S.; Shigemasa, K.; Parmley, T. H.; Parham, G. P.; O'Brien, T. J. Hepsin, a cell surface serine protease identified in hepatoma cells, is overexpressed in ovarian cancer. *Cancer Res.* **1997**, *57* (14), 2884−2887.
(74) Anisowicz, A.; Sotiropoulou, G.; Stenman, G.; Mok, S.; Sager, R. A novel protease homolog differentially expressed in breast and ovarian cancer. *Mol. Med.* **1996**, *2* (5), 624−636.
(75) Da Rocha, A. B.; Lopes, R. M.; Schwartsmann, G. Natural products in anticancer therapy. *Curr. Opin. Pharmacol.* **2001**, *1* (4), 364−369.
(76) Reddy, L.; Odhav, B.; Bhoola, K. Natural products for cancer prevention: A global perspective. *Pharmacol. Ther.* **2003**, *99* (1), 1−13.
(77) Crowell, P. L.; Kennan, W. S.; Haag, J. D.; Ahmad, S.; Vedejs, E.; Gould, M. N. Chemoprevention of mammary carcinogenesis by hydroxylated derivatives of d-limonene. *Carcinogenesis* **1992**, *13* (7), 1261−1264.
(78) Smith, O. W.; Wade, A.; Dean, F. Uroterpenol, a pettenkofer chromogen of dietary origin and a common constituent of human urine. *J. Endocrinol.* **1969**, *45* (1), 17−28.
(79) Adlercreutz, H.; Mousavi, Y.; Clark, J.; Höckerstedt, K.; Hämäläinen, E.; Wähälä, K.; Mäkelä, T.; Hase, T. Dietary phytoestrogens and cancer: *in vitro* and *in vivo* studies. *J. Steroid Biochem. Mol. Biol.* **1992**, *41* (3), 331−337.
(80) Ingram, D.; Sanders, K.; Kolybaba, M.; Lopez, D. Case-control study of phyto-oestrogens and breast cancer. *Lancet* **1997**, *350* (9083), 990−994.
(81) Scambia, G.; Ranelletti, F.; Panici, P. B.; Piantelli, M.; Bonanno, G.; De Vincenzo, R.; Ferrandina, G.; Rumi, C.; Larocca, L.; Mancuso, S. Inhibitory effect of quercetin on OVCA 433 cells and presence of type II oestrogen binding sites in primary ovarian tumours and cultured cells. *Br. J. Cancer* **1990**, *62* (6), 942.
(82) Ye, B.; Aponte, M.; Dai, Y.; Li, L.; Ho, M.-C. D.; Vitonis, A.; Edwards, D.; Huang, T.-N.; Cramer, D. W. *Ginkgo biloba* and ovarian cancer prevention: Epidemiological and biological evidence. *Cancer Lett.* **2007**, *251* (1), 43−52.
(83) Kanehisa, M.; Goto, S. KEGG: Kyoto encyclopedia of genes and genomes. *Nucleic Acids Res.* **2000**, *28* (1), 27−30.
(84) Caspi, R.; Altman, T.; Billington, R.; Dreher, K.; Foerster, H.; Fulcher, C. A.; Holland, T. A.; Keseler, I. M.; Kothari, A.; Kubo, A. The MetaCyc database of metabolic pathways and enzymes and the BioCyc collection of Pathway/Genome Databases. *Nucleic Acids Res.* **2014**, *42* (D1), D459−D471.

DOI: 10.1021/pr5009948
J. Proteome Res. 2015, 14, 917−927